CRACKING AND DUCTILITY ANALYSIS OF STEEL FIBER REINFORCED PRESTRESSED CONCRETE BEAMS IN FLEXURE

Suhas S Joshi, Nikesh Thammishetti, S Suriya Prakash, Saumitra Jain

Biography:

Suhas S Joshi is a graduate student at structural engineering division in the Department of Civil Engineering, Indian Institute of Technology Hyderabad, India. His research interests include understanding the behavior of reinforced and prestressed concrete and use of FRP composites in construction.

Nikesh Thammishetti is a research scholar at the structural engineering division, Indian Institute of Technology Hyderabad, India. He received his B.Tech from Kakatiya Institute of Technology and Science Warangal, India and Master's degree from Birla Institute of Technology Pilani (BITS Pilani). His research interests include mechanics of reinforced concrete, repair, and rehabilitation of reinforced concrete structures using innovative ductile materials.

Dr. S. Suriya Prakash is currently an Associate Professor at Department of Civil Engineering, Indian Institute of Technology Hyderabad, India. He is a recipient of prestigious Ramanujan fellowship from the Government of India. Before joining IIT Hyderabad, he worked as a design engineer at Structural Inc., Baltimore, USA. He received his Ph.D. from Missouri University of Science and Technology, USA. His research interests include seismic design, repair, and rehabilitation of reinforced concrete and masonry structures using advanced construction materials.

Saumitra Jain is a graduate student at structural engineering division in the Department of Civil Engineering, Indian Institute of Technology Hyderabad, India. He received his B.E from SGSITS Indore, India. His research interests include the behavior of reinforced concrete members, structural health monitoring of concrete members and strengthening of concrete members using FRP composites.

ABSTRACT

The present study focuses on understanding the effect of steel fiber dosage on cracking and ductile behavior of prestressed concrete beams (PCB) under flexure using digital image correlation (DIC). Seven prestressed concrete beams were cast and tested under a shear span to depth (a/d) ratio of five to simulate the flexure/flexure-shear dominant behavior. Full field strain measurement with DIC technique was used to understand the effectiveness of steel fibers on the crack bridging mechanisms. Three different volumetric fiber reinforcement ratios viz. 0.35%, 0.70% and 1.0% were considered. Test results revealed that the strain energy based ductility increased with an increase in fiber dosage from 0.35% to 1.0%. Post-cracking stiffness improved by 50% due to the addition of 1.0% volume of steel fiber dosage. DIC measurements of displacements and strains were found to be in good agreement with the conventional linear variable displacement transducer (LVDT) measurements. DIC results clearly established the effect of fibers on crack bridging and strain reduction. Concrete strains and the strain in the prestressing strand reduced due to the better crack bridging of steel fibers.

Keywords: Crack Bridging; Digital Image Correlation (DIC); Ductility; Prestressed Concrete Beams; Steel Fibers;

INTRODUCTION

Usage of fiber reinforced concrete (FRC) has been continuously increasing in the construction industry due to its various advantages such as improvement in post-cracking stiffness, flexural toughness and ease of availability at a competitive price. Steel FRC is mainly used in the seismic resistant structures, tunnel construction, blast, and impact resistant structures where the post-cracking behavior is of major concern. ACI Building Code 318[1] permits the design engineers to use steel fiber reinforced concrete (SFRC) as a replacement to conventional shear reinforcement. However, ACI codes[1,2] mandate that SFRC beams are required to have a minimum steel fiber dosage of 0.75% in volume and compressive strength not greater than 42 MPa (6.091 ksi). This mandate is because current ACI provisions are primarily based on experimental studies on non-prestressed concrete beams with a compressive strength less than 42 MPa (6.091 ksi). However, in a prestressed concrete beam, the beneficial effect of prestressing forces could further relax the minimum required fiber volume fraction and can make the use of SFRC more economical. Thus, the focus of this investigation is to study the effect of steel fibers on cracking and ductility behavior of prestressed concrete beams under flexure/flexure-shear using full field strain measurements with digital image correlation (DIC).

A number of previous works have demonstrated the use of steel fibers as secondary reinforcement for concrete elements[3-4]. Cuenca et al.[3,4] used steel fibers to control the crack propagation in precast beams and hollow core slabs. They observed that the fibers and stirrups had a synergic effect resulting in better crack control mechanisms and enhanced tension stiffening. Fantilli et al.[5] observed the increase in ductility of fiber reinforced concrete both in tension and compression. They attributed the increase in ductility in compression to

the passive confinement provided by the steel fibers. Padmarajaih and Ramaswamy[6] predicted the crack width in partially and fully prestressed concrete beams with different dosage of steel fibers. They found that addition of fibers restricted the crack initiation and propagation, eventually leading to an increase in the ultimate flexural strength. Harajli[7] studied the bond behavior of steel fiber reinforced concrete zones under static and cyclic loading. The author noted that the addition of steel fibers improved the bond strength, reduced the damage and increased the energy dissipation capacity under cyclic loading. Sahoo et al.[8] evaluated the effect of steel fibers on the behavior of concrete beams with and without stirrups. They noted that the flexural capacity did not significantly improve when the fiber dosage was more than 0.5%. Singh[9] presented the flexural modeling of SFRC to determine the ultimate capacity, crack width of rectangular sections using strain compatibility and force equilibrium equations. Additionally, a normalized design chart for strength calculations considering the random distribution of fibers and other fiber parameters was also presented.

Fantilli et al.[10] proposed a unique function related to the post peak response of different cement based materials for numerical studies. Tiberti et al.[11] studied the influence of concrete strength on the crack development of SFRC members and found that the usage of fibers led to reduced mean crack spacing in high strength concrete (HSC) when compared to normal strength concrete (NSC). They also noted that the influence of HSC and the presence of fibers requires further research to establish a stabilized crack pattern. Job and Ramaswamy[12] developed an analytical model to predict crack width, and crack spacing of partially prestressed concrete with steel fibers considering the bond slip of longitudinal reinforcement, pull-out of fibers. Cuenca and Serna[13] observed from their experimental study on hollow core

slabs that addition of fibers increased the ultimate loads as well as improved ductility when compared with the control specimens. Marazzini et al.[14] tested individual cut beams of hollow core slabs with and without steel fibers. They observed improved post peak behavior due to fiber addition. Campione[15] presented the flexural behavior of SFRC deep beams wherein they compared the RC deep beams with and without fibers, SFRC beams exhibited improved strength and ductility through crack bridging. Abbas and Khan[16] conducted fiber pull-out tests to study Fiber-Matrix interfacial behavior of hooked end steel fiber-reinforced concrete. They concluded that ultimate pull-out load was found to increase with an increase in fiber size and embedment length. Gencturk et al.[17] used Digital Image Correlation technique (DIC) for understanding the shear behavior of prestressed concrete I-beams. They recorded the values of displacement and strain using both DIC and conventional measurements. They highlighted the need for further research in using DIC technique because of non-availability of standard algorithms to identify cracks, crack width and loss of data in the region of excessive spalling. Rimkus et al.[18] proposed an algorithm to identify the crack evolution and its spacing using digital images of reinforced concrete, which can eliminate the subjective judgment using traditional methods. The flexural cracking behavior of reinforced concrete beams made-up of plain concrete (NSC and HSC) and steel fiber reinforced high strength concrete was studied using DIC technique by Hamrat et al.[19]. The authors were able to detect the first crack with high precision and measure the crack width during the testing using DIC. They have also observed an increase in the cracking load, reduction in the crack spacing and crack width due to the presence of steel fibers.

RESEARCH SIGNIFICANCE

The research carried out in the past have confirmed that the addition of steel fibers

contributes to improved post-cracking behavior through increased ductility, multiple crack formation/crack distribution, reduced crack width and enhanced toughness properties.[16-19] Various factors like shear span to depth (a/d) ratio, compressive and tensile strengths of concrete and fiber dosage influence the performance of fiber reinforced concrete elements. However, only limited results are available on the behavior of steel fiber reinforced prestressed concrete members made of concrete with strengths higher than 50 MPa. The broad objective of this study is to investigate the influence of steel fibers on the response of prestressed concrete beams and understand its effect on the crack propagation and post-cracking behavior using full-field strain measurements with the help of DIC technique. In addition, the influence of steel fiber dosage on aspects such as crack control, energy absorption capacity and deflection is also presented.

EXPERIMENTAL INVESTIGATION

The experimental program consists of casting and testing of the full-scale prestressed concrete beams designed as per IS1343-2012[24], having length of 3.5 m (11.48ft) and cross section 200 mm (7.87 in) x 300 mm (11.81 in) containing different steel fiber dosages. Four different series of beams corresponding to fiber dosages of 0, 0.35%, 0.70% and 1.0% were cast. Two beams were tested at each fiber dosage to ensure the consistency of test results. All these beams were tested at a shear span to depth ratio (a/d) of five to ensure flexure/ flexure shear behavior. A strain energy based ductility measurement was employed to study the influence of fibers. This work is part of a larger research program on investigating the effect of various types of fibers and their combinations on the performance improvement of prestressed concrete beams under different a/d ratios. Currently, work is in progress to understand the effect of fibers on shear behavior of prestressed concrete beams at low a/d

ratio of 2.5. However, only the results pertaining to a/d =5 are presented in this manuscript. All the beams were cast on the same day and were water cured for 28 days at room temperature. The overall test matrix with study parameters is detailed in **Table 1**.

Material Properties and Behavior

Concrete

All specimens were cast in the precast plant using ready-mix concrete designed as per IS: 10262-2009[25] to have a 28-day target compressive strength of 58 MPa (8.41ksi). Blended Coarse aggregates of size 10 mm and 20 mm along with fine aggregates were used to obtain a uniform mix. Mix design details are given in **Table 2**. The unit weight of concrete was 2400 kg/m^3 (149.82 lb/ft^3). The cube strength of concrete was 62 MPa (8.99 ksi) with a standard deviation of 2.2 MPa (319.08 psi) at 28 days. The SFRC cylinders were tested using servo-controlled compression testing machine for the complete stress-strain behavior (**Fig. 1**).

Behavior of Concrete in Compression

Concrete cylinders were tested (**Fig. 1a**) to obtain the stress-strain curves with and without steel fibers. The addition of steel fibers was found to significantly improve the strength and stiffness degradation in the post-peak region with better ductility (**Fig. 1b**). Previous work of authors of this manuscript has also confirmed the same at both the room and moderate temperature exposure[26-28].

Concrete tests in Tension

The control and fiber reinforced concrete (FRC) dog-bone specimens were tested using servo-controlled hydraulic MTS fatigue testing machine under pure tension. The loading was controlled at a rate of 10 μm/min up to a mid-span displacement of 0.8 mm (0.03 in) and then

at 50 μm/min up to 1.2 mm (0.047 in) displacement followed by 1000 μm/min for the rest of the test. All the specimens with different fiber dosages were tested in uniaxial tension using rigid steel plates on a servo controlled closed loop system as shown in **Fig. 2**. The failure pattern in control specimen is predominantly due to a single explicit crack at the center of the specimen. This observation indicates that the stress concentration in the crack region reduces the post-cracking load resistance of the specimen. On the other hand, the FRC specimen showed a similar large crack at failure, but the crack opening was delayed due to the presence of fibers in the section. Similar observations have been made by Choun et al.[33] as shown in Fig.2b.

Internal reinforcement - prestressing steel strands

Two numbers of half an inch (12.7 mm diameter) strands containing seven low relaxation wires with an effective area of 200 mm^2 (0.31 in^2) were used for prestressing the beams. Coupon specimens were prepared for tendons and tested under tension using a servo-controlled machine. The ultimate tensile strength and modulus of elasticity were found to be 1860 MPa (269.77 ksi) and 196.5 GPa (28500 ksi), respectively. Jacking force is applied to each of the strands to subject them to an initial strain of 0.004.

Hooked end steel fibers

Hooked end steel fibers having length and diameter of 30 mm (1.18 in) and 0.6 mm (0.023 in), respectively (**Fig. 3**) were used in this investigation. The tensile strength and modulus of elasticity of steel fibers were found to be 1000 MPa (145 ksi) and 200 GPa (29007 ksi), respectively. During casting, the fibers were added gradually to prevent the balling effect and to obtain a uniform fiber distribution. Uniform fiber distribution was verified by the

inspection of the cracked faces of failed beams after testing.

Instrumentation

Displacements in all the specimens were recorded using Linear Variable Displacement Transducers (LVDT) and DIC. LVDTs were positioned at specific locations along the length of the beam to capture the entire curvature profile during testing. Two 100 mm (3.94 in) LVDTs were positioned at the center of the span to capture the mid-span deflection. Six LVDTs were used to form a strain rosette (**Fig. 4**) to measure surface strains near the loading point. Strain gauges of 5 mm (0.197 in) gauge length were instrumented at mid-span of the prestressing strands to capture the strain variation in the strands during testing.

Digital Image Correlation (DIC)

Digital image correlation (DIC) is a technique for measuring the whole-field strain and displacement of specimens. DIC works by comparing two images of the specimen coated with a random speckle pattern in an undeformed and deformed state[31]. Images of the object's surface before and after deformation are recorded, digitized and stored in the computer. These images are then analyzed to determine the displacements by invoking a pattern matching principle. Since it is impossible to find matching points using single pixel, areas (called as subsets) containing multiple pixels are used for the analysis[31]. The size of subset varies with respect to the experimentation details. The step size controls the density of analyzed data. For example, a step size of 5 will analyze every 5^{th} point in each direction. A higher step size gives faster results but coarser data. A smaller step size will return more points but will take more computation time. For the present experiments, a subset size of 35 and a step size of five was chosen after a thorough sensitivity analysis. All the specimens had

speckle pattern on the surface for capturing of DIC images. The surface was initially coated with non-reflective white paint, and then black speckle was sprayed on the white coat. Two halogen lights were placed at an angle to the specimen as shown in **Fig. 5** to illuminate the specimen. The camera was placed in front of the specimen with its axis normal to the specimen. Images were taken at regular intervals and were processed using specialized software (VIC- 2D) for strain analysis, crack initiation and propagation.

Test Setup and Loading Details

All beams were tested in a four-point bending configuration by which a constant moment region at the mid-span was generated. **Fig. 6** illustrates the components used in the test setup. A 250 kN (56.25 kips) MTS servo-hydraulic actuator was used to apply the loads. The actuator load is transferred to the concrete specimens through longitudinal rigid steel spreader beam and thereafter to the I-beams as shown in **Fig. 6**. Loading was applied monotonically in displacement control mode at a rate of 0.05 mm/sec. Loading was paused intermittently to observe and mark the cracks and study the failure progression.

TEST RESULTS AND DISCUSSION

Load-deflection Behavior

All the beams were tested with shear span to depth ratio of five and the load vs. mid-span deflection plots were obtained as shown in **Fig. 7**. Two specimens were tested for each fiber dosage to ensure the consistency of the results. The load – displacement behavior of PSC beams without fibers (Control Specimen) are illustrated in **Fig. 7a**. The average cracking load observed from the test was 60 kN (13.5 kips). After cracking, the beam continued to resist the applied load until 142.5 kN (32.06 kips) and the corresponding deflection was 40 mm (1.57

in). It is worth mentioning that the beam was heavily under reinforced leading to the yielding of strands just before the peak load.

The beam with 0.35% steel fibers exhibited better ductility as compared to the control specimen. About 13% improvement in cracking load and 23% (average) improvement in post-cracking stiffness was observed (**Fig. 7b**). However, the ultimate load did not change. This beam had better crack distribution with the delayed formation of cracks as compared to the control specimen before reaching its final failure load. Flexure dominant failure was observed with 0.35% steel fiber dosage. The crack bridging effect was evident through the formation of a number of smaller cracks and fewer major cracks. The specimen with 0.7% steel fiber dosage (**Fig. 7c**) exhibited better ductility than the specimen with 0.35% fiber dosage. However, there was no substantial improvement in ultimate strength due to higher fiber dosage. Additionally, significant improvement in the post-cracking stiffness (50%), ductility and ultimate load (11.6%) was observed with the increase in fiber dosage from 0% to 1.0%. The specimen had an ultimate load of 159 kN (35.77 kips) with the first crack forming at a load of 70 kN (15.75 kips). Test was terminated at 100 mm (3.94 in) displacement due to a limitation in stroke capacity of the actuator. However, the specimen could have resisted loads at even higher displacements which is evident from the overall load displacement curves (**Fig. 7d**). It was evident from the test results that presence of steel fiber increases the displacement corresponding to cracking load. The addition of fibers also converted the brittle flexure-shear failure of control beams into ductile flexure dominant failure in fiber reinforced beams. One specimen with 1.0% steel fiber dosage had honeycombing due to improper compaction and hence it was excluded from comparisons.

Crack distribution and failure modes

The crack distribution of tested specimens is illustrated in **Fig. 8**. For control specimens, the first flexural crack occurred at the tension fiber in the constant moment region. Soon after cracking, the formation of multiple cracks continued at the mid-span location below the loading point. All the specimens failed in flexure mode except the control specimen which failed in the flexure-shear mode soon-after the yielding of prestressing strands. The failure mode in control specimen was sudden due to the crushing of concrete just after the yielding of strands. The presence of steel fibers resulted in more distribution of cracks and converted sudden brittle failure to a gradual ductile failure mode.

Load vs. Strain Behavior

Strain gauges were installed on the strand at the mid length of the specimen to measure the strain variation during pre-tensioning and testing. Strain gauges recorded the value of around 4000 μm/m during pre-tensioning. Load vs. strain graphs presented in **Fig. 9** shows a trilinear behavior. The first change in slope can be attributed to the cracking of beam. The second change in slope can be correlated to the beginning of crushing of concrete in compression. **Fig. 9** indicates that strain in the strands was nominal before cracking. After cracking, as expected, the strain increased significantly indicating the higher contribution of strands in load resistance. In general, the strain values at particular load reduced with an increase in fiber dosage indicating the steel fiber contribution in load resistance after cracking (Fig. 9). The strands yielded in all the specimens before they could reach their ultimate load. However, strain values were not recorded after a certain load value level due to malfunctioning of the strain gauges.

Fiber Distribution on the fractured surface

The fiber distribution on the cracked section was verified after testing of PSC beams to complete failure. **Fig. 10** shows the distribution of steel fibers on the failure surface. It presents the random and uniform distribution of fibers along the depth of the section. Moreover, the elongation of fibers and fiber pull–out (bond failure) illustrates the contribution of fibers in load resistance. Nevertheless, the fiber contribution in crack bridging was evident from the fractured surfaces of the failed beams.

Energy Absorption capacity

The strain energy developed to resist the applied external load was calculated for comparison. Energy absorption capacity of PSC beams can be obtained from the area under load - deflection curve. All the specimens were tested at same a/d ratio but with different fiber dosages. Their energy absorption capacity is compared and is presented in **Table 3**. The addition of steel fibers resulted in an increase of energy absorption capacity due to better crack bridging. Energy capacity doubled when 1.0% by volume of steel fibers were added to the control specimen.

ANALYSIS OF RESULTS USING DIGITAL IMAGE CORRELATION

Load vs. Deflection analysis

Displacements and strains from DIC analysis can be correlated only until major crack formation. After significant cracking, the correlation breaks due to excessive cracking and spalling of concrete leading to the difficulty in pattern matching. The load - deflection response of the specimens using DIC analysis is compared with the LVDT measurements for beams with different fiber dosages (**Fig. 11**). The results from DIC analysis showed a close

agreement with the LVDT measurements.

Effect of fibers on the tensile strain in concrete

Full field strains on the surfaces were measured using the VIC-2D software. Strain distribution was evaluated to see the effect of steel fiber contribution in resisting the crack propagation. A horizontal line a-b was chosen (**Fig. 12a**) in the tensile zone of all the tested beams. **Fig. 12b** shows the tensile strain variation along the line a-b at a load level of 60kN (13.48 kips), which is slightly less than the cracking load. It indicates that the peak strain along the considered horizontal line is same for beams of different series. This elucidates the fact that fibers do not play a vital role in load carrying mechanisms before cracking. On the other hand, **Fig. 12c** shows the tensile strain variation along line a-b at a load of 70 kN (15.73 kips), which is greater than the cracking load. It presents the decrease in peak strain at same load level after cracking with the increase in fiber dosage. The reduction in strain indicates that fibers resist the crack widening, localization and helps to redistribute the stresses and increase the number of cracks. The extent of reduction in strains mainly depends on the dosage of steel fibers. In the **Fig. 12a-c** a sudden jump in the strain contour indicates the presence of a crack in that region. **Fig. 13** illustrates the reduction in average strain along the level of crack tip at failure due to addition of fiber. Additionally, **Fig. 13** also indicates that the presence of steel fiber reduces the maximum strain as much as by 50%. The strain values corresponding to the post-cracking loads for different specimen highlights that the presence of steel fibers reduces the strain at the crack locations (**Fig. 14**) .

PREDICTIONS USING ANALYTICAL MODELS

The behavior of SFRC under compressive and tensile loads are predicted theoretically based

on the models available in literature[32, 34, 35]. The following sections discuss the methodology followed to obtain the constitutive relationships of SFRC. Later, the models developed are utilised to perform the moment-curvature analysis of the section considered in this research.

Constitutive relationships for SFRC under Compression

Several analytical models are available in the literature to predict the behavior of SFRC under compression. Ou et al.[34] proposed an analytical model for the development of compressive stress-strain relationship of SFRC, which is an extension of the stress - strain model previously proposed by Carreira and Chu[32] for plain concrete under compression:

$$\frac{\sigma_c}{f'_{cf}} = \frac{\beta\left(\frac{\varepsilon_c}{\varepsilon_{cf}}\right)}{\beta - 1 + \left(\frac{\varepsilon_c}{\varepsilon_{cf}}\right)^{\beta}} \quad (1)$$

in which σ_c is compressive stress; f'_{cf} is the compressive strength; ε_{cf} is the peak strain; ε_c is the compressive strain, and β defines the shape of the stress-strain curve which is a function of the reinforcement index (RI_v).

$$f'_{cf} = f'_c + 2.35(RI_v) \quad (2)$$

$$\varepsilon_{cf} = \varepsilon_{co} + 0.0007(RI_v) \quad (3)$$

$$\beta = 0.71(RI_v)^2 - 2.00(RI_v) + 3.05 \quad (4)$$

$$RI_v = V_f \frac{l}{\phi} \quad (5)$$

f'_c, ε_{c0} are compressive strength (in MPa) and the strain (mm/mm) at the peak stress of plain concrete; V_f , l , ϕ are volume fraction of fibers (in %), length and diameter of fibers, respectively.

The cylinder compressive strength (43 MPa) of control specimen is used for the development of stress-strain behavior of SFRC with different volume fraction of fibers employing the model defined by equations 1-5.

Constitutive relationships for SFRC under Tension

The tensile behavior of SFRC usually depends on the strength of the plain concrete, type of fiber and fiber fraction. Neocleous et al.[35] developed an analytical model to predict the behaviour of SFRC under tension, adopting recommendations of RILEM[36] for predicting the tensile strength of plain concrete. Typical behavior of SFRC is shown in the **Fig. 15.**

Various salient points in the tensile constitutive relationships for SFRC are computed as follows:

$$f_c^{'} = 0.8 * (f_{ck}) \quad (6)$$

$$f_{ctm} = 0.3 * (f_c^{'})^{\frac{2}{3}} \quad (7)$$

$$f_{fcm} = f_c^{'} + k_x S_p \quad (8)$$

$$E_c = 9500 * (f_{fcm})^{\frac{2}{3}} \quad (9)$$

$$\sigma_1 = 0.7 * f_{ctm} * \frac{(1600 - d)}{1000} \quad (10)$$

$$\sigma_{1f} = \sigma_1 * (1 + 0.32 * V_{fw}) \quad (11)$$

$$\sigma_{2f} = \sigma_{1f} * e^{\xi(\varepsilon_1 - 0.002)10^3} \quad (12)$$

$$\sigma_{3f} = 0 \quad (13)$$

$$\varepsilon_{1f} = \frac{\sigma_{1f}}{E_c} \quad (14)$$

$$\varepsilon_{2f} = \varepsilon_{1f} + \left(\frac{2}{1000}\right) \quad (15)$$

$$\varepsilon_{3f} = 0.04 \quad (16)$$

Where f_{ck} , f_c' are the characteristic compressive strength of cube and cylinder (in MPa) respectively; f_{ctm} , f_{fcm} , E_c are the characteristic tensile strength, mean tensile strength and mean secant modulus of concrete (in MPa); V_{fw} is the weight fraction of fibers (in %); σ_{1f}, σ_{2f}, σ_{3f} are the salient points of the tensile stress–strain model corresponding to strains of ε_{1f}, ε_{2f}, ε_{3f} respectively.

Moment Curvature Analysis

A layer-by-layer method of sectional analysis was carried out to establish the moment-curvature behavior of steel fiber reinforced prestressed concrete sections using an iterative procedure. To maximize the accuracy of the results and to minimize the computational effort, the cross section and corresponding stress-strain curves were discretized into a number of layers of small thickness so as to get the uniform strain throughout the thickness **(Fig. 16)**. The constitutive relationship for fiber reinforced concrete in compression and tension according to the model[34, 35] **(Fig. 15)** is used. A compressive top fiber strain value is fixed, and the neutral axis depth is iterated to satisfy the force equilibrium. Moment resistance is calculated from the moment equilibrium, and the corresponding curvature can be arrived using the assumed top compressive strain and the neutral axis depth.

The analytical results are compared with experimentally measured moment-curvature response in **Fig. 17**. It can be observed that post cracking stiffness and ultimate strength

increases with increase in fiber dosage. The cracking and ultimate moment were found to be matching reasonably well with the test results **(Fig. 17)**. However after certain loading curvature was not measured due to instrumentation error. Hence overall response was not presented. RILEM recommendations[36] were also utilized to compare the experimental results at ultimate capacity as shown in **Table.3**.

SUMMARY AND CONCLUSIONS

Pre-tensioned prestressed concrete beams with and without steel fibers were cast and tested four point bending to evaluate the role of steel fibers in crack bridging and improvement in serviceability performance. Based on the test results of seven prestressed concrete beams presented in this study, the following major conclusions can be drawn:

i) Though the addition of steel fibers showed marginal improvement in the peak strength, it resulted in very good improvement in strain energy based ductility of the prestressed concrete beams. The major contribution of steel fibers was in bridging the cracked surfaces which resulted in improved post-cracking stiffness and higher ultimate deflection. The strain in the strand reduced due to the addition of steel fibers in the post-cracking regime.

ii) Distribution of cracks increased with increase in the addition of steel fibers. More importantly, the failure mode changed from flexure-shear to flexure resulting in higher ductility and ultimate deflections.

iii) No increase in ultimate flexural strength was observed at low fiber dosages. The maximum increase in load capacity was about 11.6% at a higher fiber dosage of 1.0%.

iv) Energy dissipation capacity increased with increase in fiber dosage. It doubled when 1.0% by volume of steel fibers was added.

v) DIC measurements correlated well with conventional measurements of displacement sensors. The reduction in peak strain in tensile fibers was up to 50% due to the crack bridging mechanism of steel fibers.

ACKNOWLEDGEMENTS

This experimental work was carried out as part of the project funded through Utchattar Avishkar Yojana Scheme of Indian Government. PRECA India Pvt. Ltd. and Grenix India Ltd., donated the materials required for this research. PRECA provided the labor required for the casting of specimens in their factory. All of their support is duly acknowledged.

REFERENCES

1. ACI 318. "Building code requirements for structural concrete". American Concrete Institute 2011; Farmington Hills (MI): USA.
2. ACI 544. "State of the Art Report on Fiber Reinforced Concrete". American Concrete Institute 2002; Farmington Hills (MI): USA.
3. Cuenca, E., Echegaray-Oviedo, J., and Serna, P. (2015). "Influence of concrete matrix and type of fiber on the shear behavior of self-compacting fiber reinforced concrete beams". *Composites Part B: Engineering*, 75, 135-147.
4. Cuenca, E., and Serna, P. (2013). "Shear behavior of prestressed precast beams made of self-compacting fiber reinforced concrete". *Construction and Building Materials*, 45, 145-156.
5. Fantilli, A. P., Mihashi, H., Vallini, P., and Chiaia, B. M. (2011). "Equivalent Confinement in HPFRCC Columns Measured by Triaxial Test". *ACI Materials Journal*, 108(2), 159-167.
6. Padmarajaiah, S. K., and Ramaswamy, A. (2004). "Flexural strength predictions of steel fiber reinforced high-strength concrete in fully/partially prestressed beam specimens*". Cement and Concrete Composites*, 26(4), 275-290.
7. Harajli, M. H. (2010). "Bond behavior in steel fiber-reinforced concrete zones under

static and cyclic loading: experimental evaluations and analytical modelling". *Journal of Materials in Civil Engineering*, 22(7), 674-686.

8. Sahoo, D. R., Bhagat, S., and Reddy, T. C. V. (2016). "Experimental study on shear-span to effective-depth ratio of steel fiber reinforced concrete T-beams". *Materials and Structures*, 49(9), 3815-3830.

9. Singh, H. (2014). "Flexural modeling of steel fiber-reinforced concrete members: analytical investigations". *Practice Periodical on Structural Design and Construction*, 20(4), 04014046.

10. Fantilli, A. P., Mihashi, H., and Vallini, P. (2007). "Post-Peak Behaviour of Cement-Based Materials in Compression". *ACI Materials Journal*, 104,501-510.

11. Tiberti, G., Minelli, F., Plizzari, G. A., and Vecchio, F. J. (2014). "Influence of concrete strength on crack development in SFRC members". *Cement and Concrete Composites*, 45, 176-185.

12. Job, T., and Ramaswamy, A. (2006). Crack width in partially prestressed T-beams having steel fibers. *ACI structural journal,* 103(4), 568.

13. Cuenca, E., and Serna, P. (2013). "Failure modes and shear design of prestressed hollow core slabs made of fiber-reinforced concrete". *Composites Part B: Engineering*, 45(1), 952-964.

14. Marazzini, M., and Rosati, G. (1999). "Fiber reinforced high-performance concrete beams material and structural behavior". *ACI Special Publication*, 182, 29-52.

15. Campione, G. (2011). "Flexural behavior of steel fibrous reinforced concrete deep beams". *Journal of Structural Engineering*, 138(2), 235-246.

16. Abbas, M. Y., and Khan, M. I. (2016). "Fiber-matrix interfacial behavior of hooked-end steel fiber-reinforced concrete". *Journal of Materials in Civil Engineering*, 28(11), 04016115.

17. Gencturk, B., Hossain, K., Kapadia, A., Labib, E., and Mo, Y. L. (2014). "Use of digital image correlation technique in full-scale testing of prestressed concrete structures". *Measurement*, 47, 505-515.

18. Rimkus, A., Podviezko, A., Gribniak, V. (2015). "Processing digital images for crack localization in reinforced concrete members". *Procedia Eng*, 122, 239-43.

19. Hamrat, M., Boulekbache, B., Chemrouk, M., Amziane, S. (2016). "Flexural cracking behavior of normal strength, high strength and high strength fiber concrete beams, using Digital Image Correlation technique". *Construction and Building Materials*, 106, 678-92.

20. Narayanan, R., and Darwish, I. Y. S. (1987). "Shear in prestressed concrete beams containing steel fibres". *International Journal of Cement Composites and Lightweight Concrete*, 9(2), 81-90.

21. Peaston, C., Elliot, K., and Paine, K. (1999). "Steel fiber reinforcement for extruded prestressed hollow core slabs". *ACI Special Publication*, 182, 87-108.

22. Barros, J. A., and Figueiras, J. A. (1999). "Flexural behavior of SFRC: testing and modelling". *Journal of Materials in Civil Engineering*, 11(4), 331-339.

23. Soulioti, D. V., Barkoula, N. M., Paipetis, A., and Matikas, T. E. (2011). "Effects of fibre geometry and volume fraction on the flexural behaviour of steel- fibre reinforced concrete". *Strain*, 47, e535-e541.

24. IS 1343, "Code of Practices for Prestressed Concrete," Bureau of Indian Standards, New Delhi, India, 1980, 62 pp.

25. IS 10262 "Proportioning-Guideline, Indian Standard Concrete Mix". Bureau of Indian Standards, New Delhi, 2009.

26. Rasheed, M. A., and Prakash, S. S. (2015). "Mechanical behavior of sustainable hybrid-synthetic fiber reinforced cellular light weight concrete for structural applications of masonry". *Construction and Building Materials*, 98, 631-640.

27. Jain, S., Prakash, S. S., and Subramaniam, K. V. L. (2016). "Monitoring of concrete cylinders with and without steel fibers under compression using piezo-ceramic smart aggregates". *Journal of Nondestructive Evaluation*, 35(4), 59.

28. Srikar, G., Goudar, A.G., and Prakash, S. S. (2016). "A study on residual compression behavior of structural fiber reinforced concrete exposed to moderate temperature using digital image correlation". *International Journal of Concrete Structures and Materials*, 10(1), 75-85.

29. Carreira, D. J., and Chu, K. H. (1986). "Stress-strain relationship for reinforced concrete in tension". *ACI Journal*, 83(1), 21-28.

30. Olivito, R. S., and Zuccarello, F. A. (2010). "An experimental study on the tensile

strength of steel fiber reinforced concrete". *Composites Part B: Engineering*, 41(3), 246-255.

31. Schreier, H., Orteu, J. J., and Sutton, M. A. (2009). "Image correlation for shape, motion and deformation measurements". Springer, US.
32. Carreira, D. J., and Chu, K. H. (1985). "Stress-strain relationship for plain concrete in compression". *ACI Journal*, 82(6), 797–804.
33. Choun, Y. S., and Park, H. K. (2015). "Containment performance evaluation of prestressed concrete containment vessels with fiber reinforcement". *Nuclear Engineering and Technology*, 47(7), 884-894.
34. Ou, Y., Tsai, M., Liu, K., and Chang, K. (2011). "Compressive behavior of steel-fiber reinforced concrete with a high reinforcing index." *J. Mater. Civ. Eng.*, 24(2), 207–215.
35. Neocleous, K., Tlemat, H., and Pilakoutas, K. (2006). "Design issues for concrete reinforced with steel fibers." *J. Mater. Civ. Eng.*, 18(5), 677–685.
36. RILEM TC 162-TDF (2002). "Test and design methods for steel fibre reinforced concrete". *Materials and structures*, 35(9), 579-582.

TABLES AND FIGURES

List of Tables:

Table 1 - Details of Test Specimens
Table 2 - Mix Design Details
Table 3 - Summary of Test results

List of Figures:

Fig. 1 *– Cylinder testing under compression*

Fig. 2 *- Testing of FRC specimen under pure tension*

Fig. 3 *- Hooked end steel fibers*

Fig. 4 *- Instrumentation details: LVDT and strain rosette arrangement*

Fig. 5 *- Schematic plan view of DIC setup*

Fig. 6 *- Experimental setup and instrumentation for prestressed concrete beams*

Fig. 7 *- Comparison of Load-Deflection behavior*

Fig. 8 *- Crack distribution and failure modes*

Fig. 9 *- Effect of steel fibers on strain variation of strands in PCB*

Fig. 10 *- Steel fibers distribution on the failure surface*

Fig. 11 *- Comparison of DIC results with the LVDT measurement*

Fig. 12 *- Longitudinal strain contours (DIC) on the horizontal line a-b before and after cracking*

Fig. 13 *- Average Strain along the level of crack tip -at failure*

Fig. 14 *- DIC images showing strain contours at various load levels*

Fig. 15 *- Stress-strain response of fiber-reinforced concrete in compression and tension*

Fig. 16 *- Layer by layer approach for sectional analysis*

Fig. 17 *- Comparison of Analytical and Experimental results*

Table 1: Details of Test Specimens

Specimen Number	Label	Fiber content (Volume fraction in %)	a/d	Compressive Strength of cube (fck) in MPa (ksi)
1	SF00-1	0		
2	SF00-2	0		
3	SF35-1	0.35		
4	SF35-2	0.35	5	62 (8.99)
5	SF70-1	0.7		
6	SF70-2	0.7		
7	SF100-2	1.0		

Table 2: Mix Design Details

Material	Quantity (kg/m^3)
20 mm aggregate	754 kg
10 mm aggregate	355 kg
Crushed Stone Sand (CSS)	415 kg
Natural River Sand (NRS)	313 kg
Cement (OPC 53)	428 kg
Flyash	22 kg
Water	165 kg
Admixture	2.5 kg

($16.01\ kg/m^3 = 1\ lb/ft^3$, 1 kg= 2.2 lb)

Table 3: Summary of Test results

Specimen	SF00-1	SF00-2	SF35-1	SF35-2	SF70-1	SF70-2	SF100-2
Cracking load, Pcr , kN (kip)	55 (12.36)	66 (14.84)	68 (15.28)	70 (15.73)	70 (15.73)	67 (15.06)	70.3 (15.80)
Deflection at Cracking load, Δcr ,mm (in)	2.5 (0.098)	2.97 (0.117)	3.02 (0.119)	3.28 (0.13)	4.03 (0.158)	4.02 (0.158)	4.66 (0.183)
Peak load, Ppl ,kN (kip)	141 (31.7)	144 (32.37)	143 (32.14)	143.5 (32.26)	148.6 (33.4)	146 (32.82)	159 (35.75)
Increase in Ppl (%)	-	-	0.35	0.7	4.28	2.45	11.57
Deflection at peak load, Δpl ,mm (in)	36.65 (1.44)	42.2 (1.66)	34.4 (1.35)	29.6 (1.17)	45.0 (1.77)	32.4 (1.27)	36.6 (1.44)
Mid span deflection at failure, mm (in)	65.0 (2.56)	53.3 (2.09)	97.5 (3.83)	78.8 (3.10)	99.0* (3.89)	97.8* (3.85)	99.7* (3.92)
Post cracking stiffness , kN/mm (kips/in)	2.57 (14.73)	2.59 (14.79)	2.903 (16.578)	3.457 (19.744)	3.076 (17.567)	3.335 (19.046)	3.871 (22.107)
Increase in Post cracking stiffness (%)	-	-	12.54	34.03	19.26	29.3	50.07
Experimental- cracking moment , kN-m (lb-ft)	34.4 (25372)	37.5 (27658)	42.5 (31346)	43.7 (32231)	43.7 (32231)	41.9 (30903)	43.9 (32378)
Experimental- peak moment , kN-m (lb-ft)	88.1 (64979)	89.4(65938)	89.4 (65938)	89.7 (66159)	92.9 (68519)	91.3 (67339)	99.4 (73313)
Cracking moment(RILEM),kN-m(lb-ft)	34.7(25593)		39(28764)		43.3(31936)		46.7(34444)
Peak moment(RILEM),kN-m(lb-ft)	81(59742)		86(63430)		91(67118)		95(70068)
Strain Energy (Joule)	6332	6358	9309	10989	11534	11774	13239
% increase in strain energy	-	-	46.7	73.2	81.8	85.6	108.7

* Test was terminated due to limitation in stroke capacity of the actuator

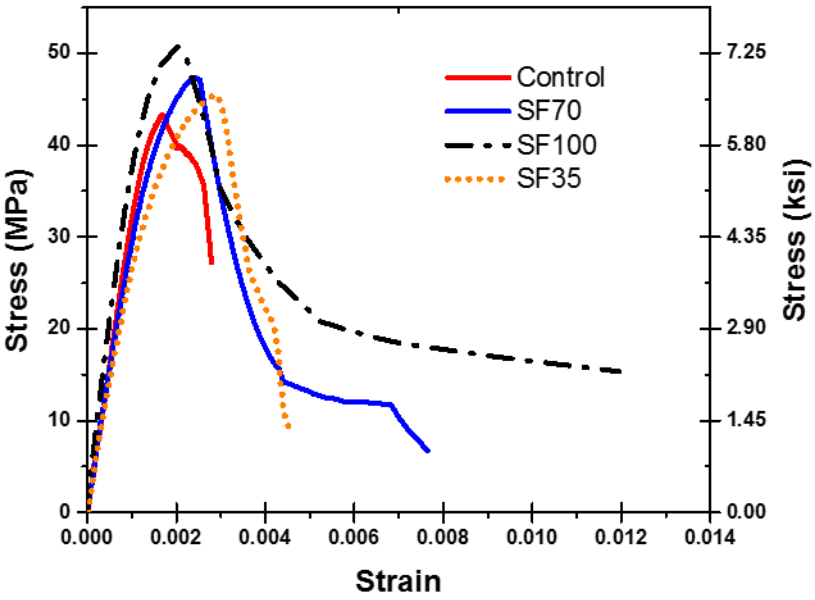

1

2 *(a) Test Setup* *(b) Stress strain curves Control vs. FRC*

3 *Fig. 1: Cylinder testing under compression.*

4

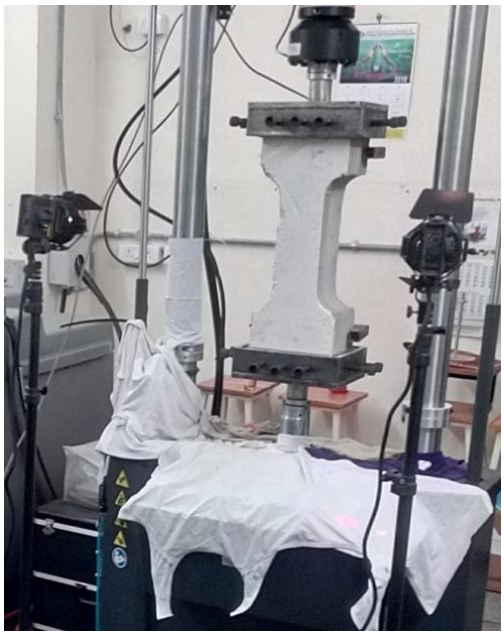

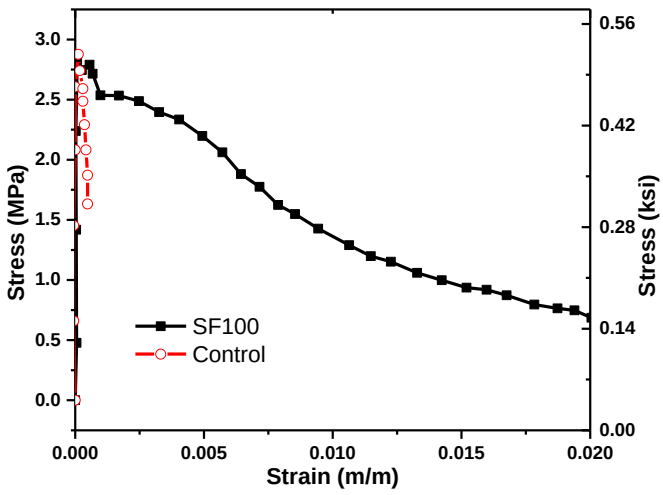

5

6 *(a) Test setup* *(b) FRC behavior under uniaxial tension*[33]

7 Fig. 2: *Testing of FRC specimen under pure tension*

8

Fig. 3: *Hooked end steel fibers*

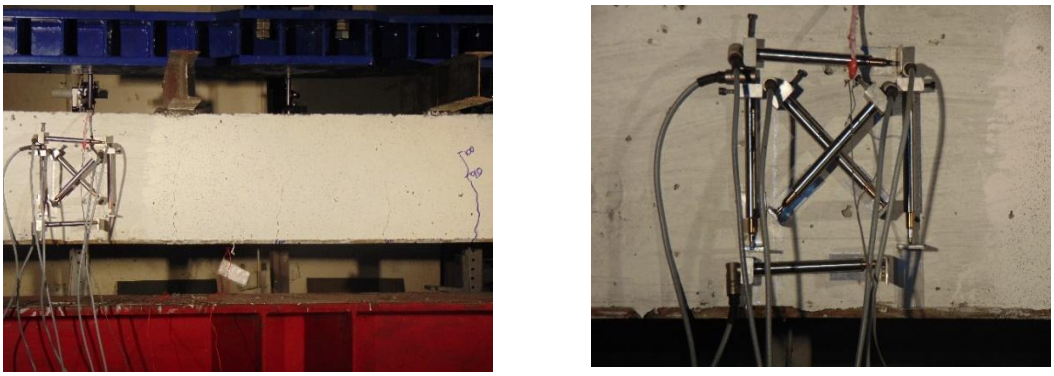

Fig. 4: *Instrumentation details: LVDT and strain rosette arrangement*

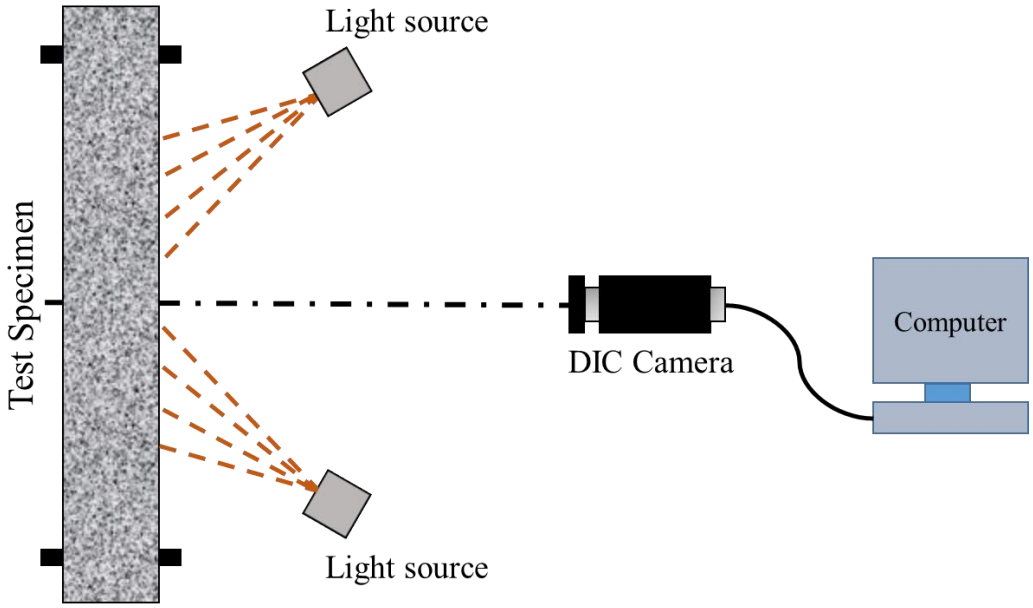

Fig. 5: *Schematic plan view of DIC setup*

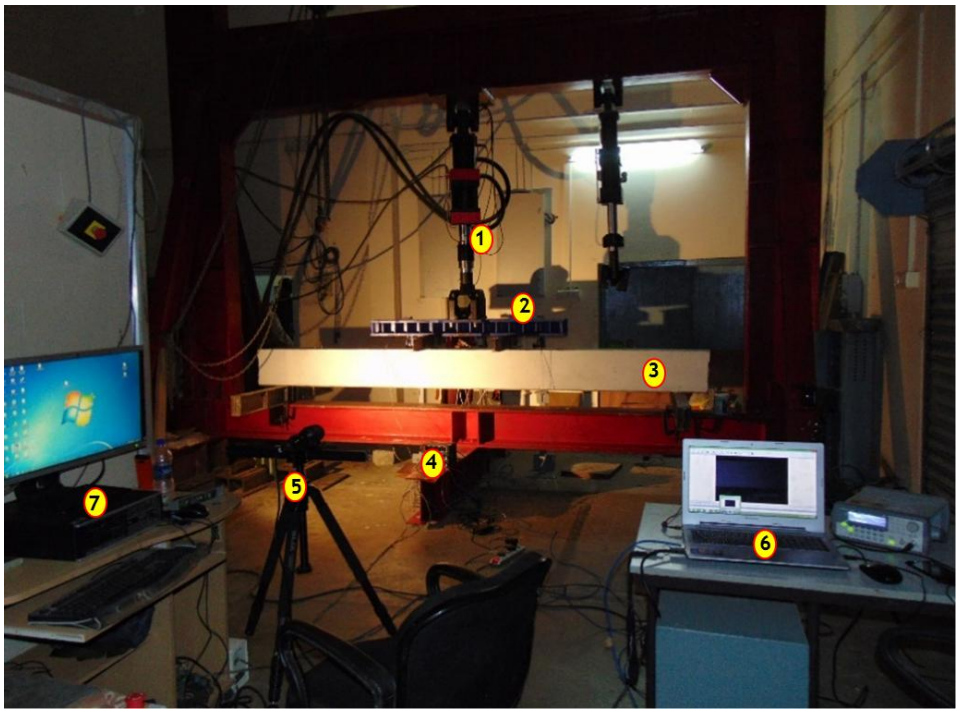

1. 250 kN MTS Actuator; **2**. Spreader Beam; **3**. PSC Beam; **4**. HBM DAQ system; **5**. DIC camera; **6**. Laptop; **7**. MTS Controls system.

a) *Test setup and instrumentation details*

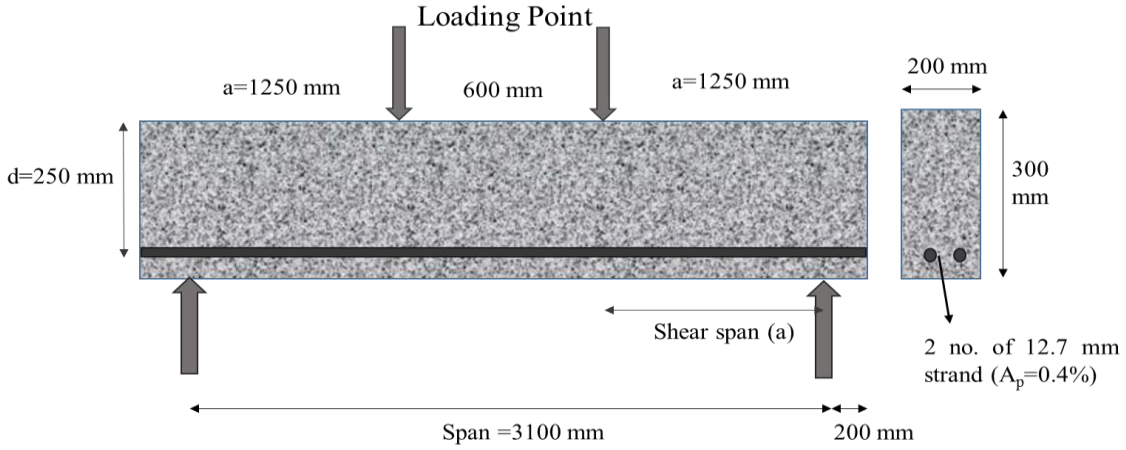

b) *Schematic of loading and Sectional Details (25.4 mm = 1 in)*

Fig. 6: *Experimental setup and instrumentation for prestressed concrete beams*

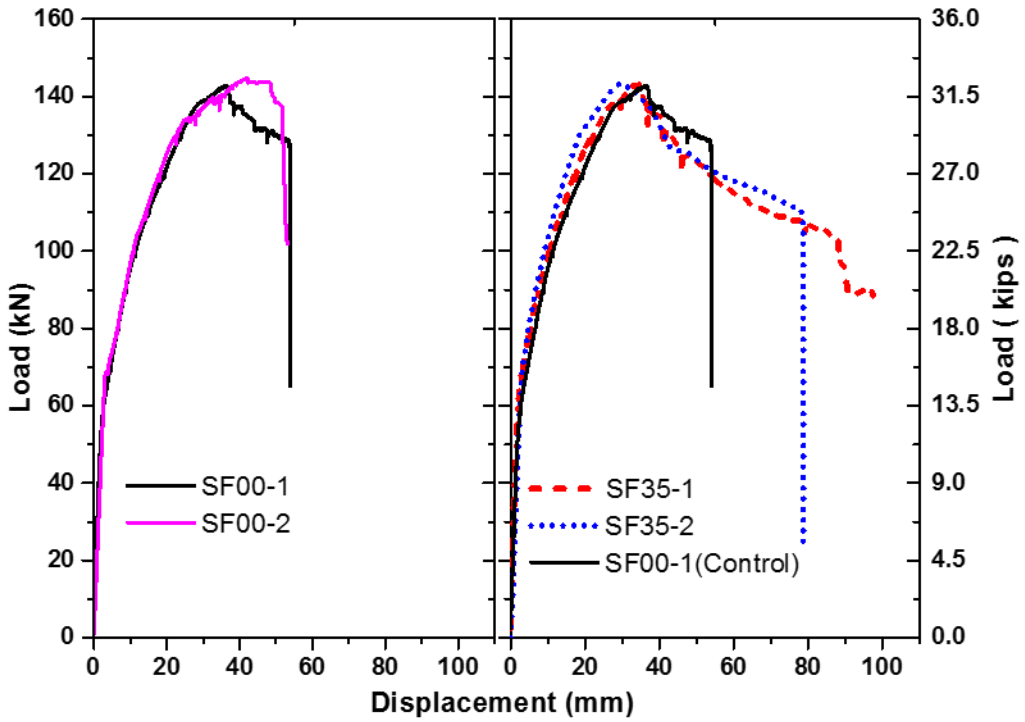

a) *Control specimen (without fibers)* b) *PCB with 0.35% of Steel Fibers*

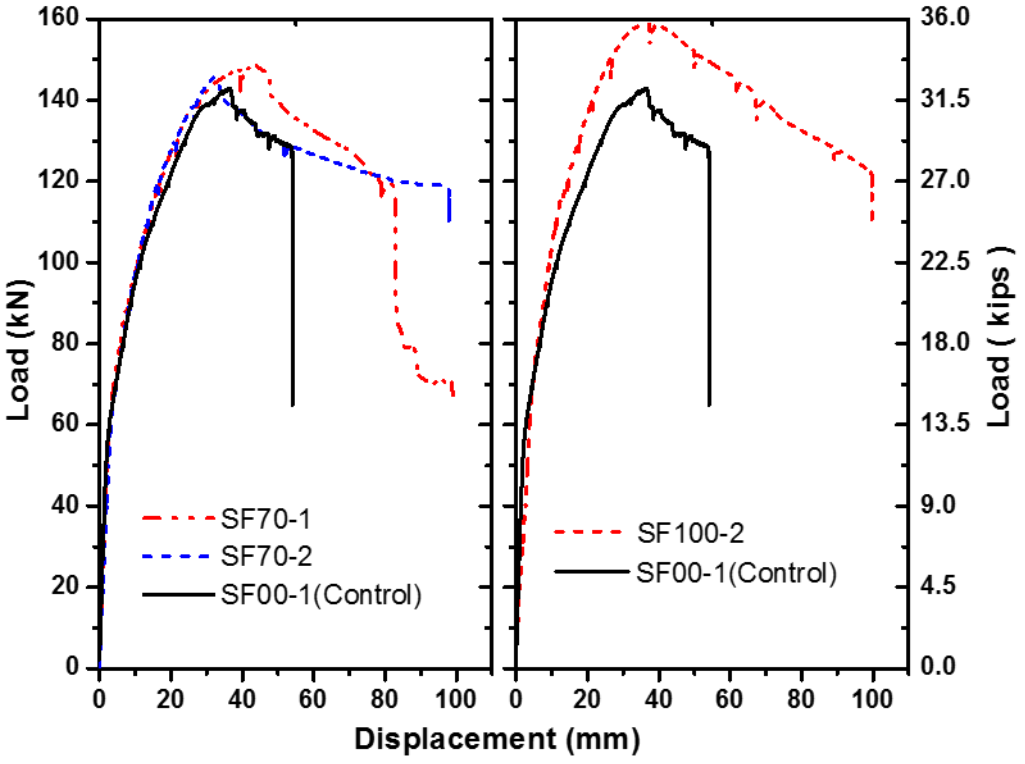

c) *PCB with 0.7% of Steel Fibers* d) *PCB with 1.0% of Steel Fibers*

Fig. 7*: Comparison of Load-Deflection behavior*

1

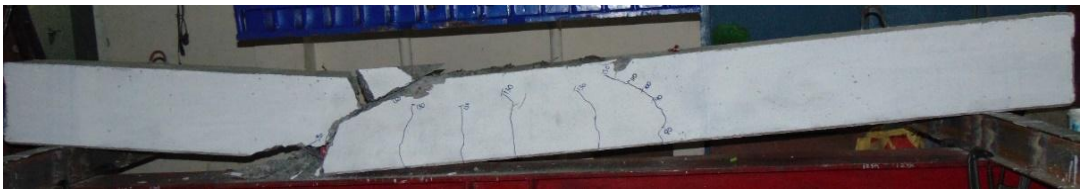

(a) *Control specimen*

(b) *SF-0.35%*

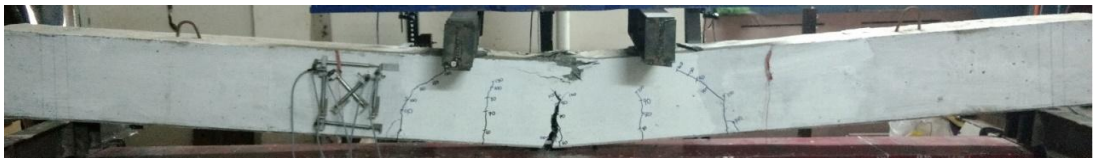

(c) *SF-0.7%*

(d) *SF-1.0%*

Fig. 8: *Crack distribution and failure modes*

2
3
4

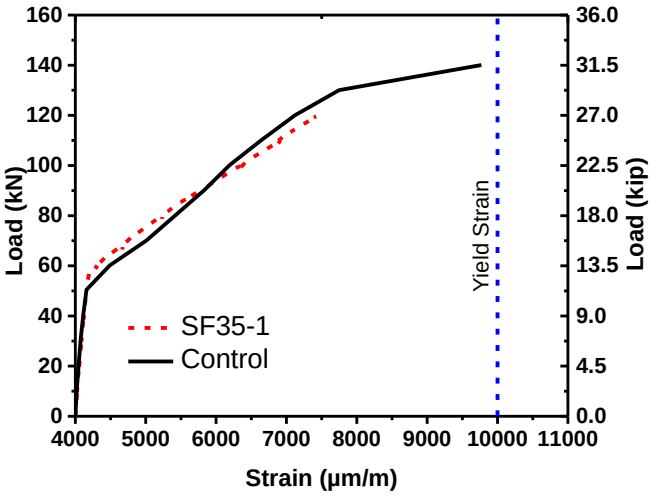

(a) *Strand strain variation in SF35 and SF00*

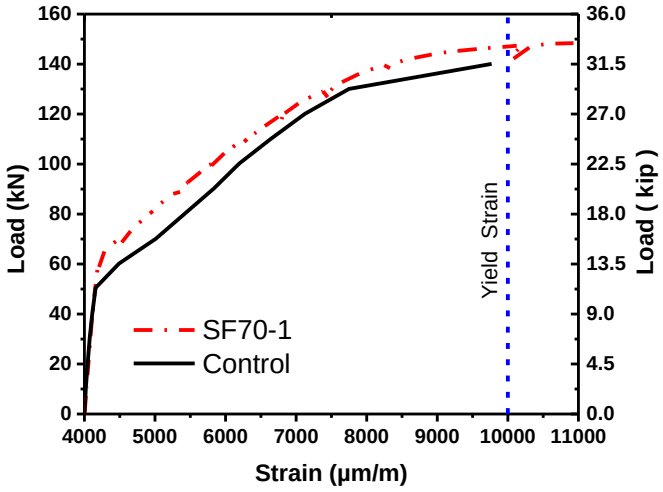

(b) *Strand strain variation in SF70 and SF00*

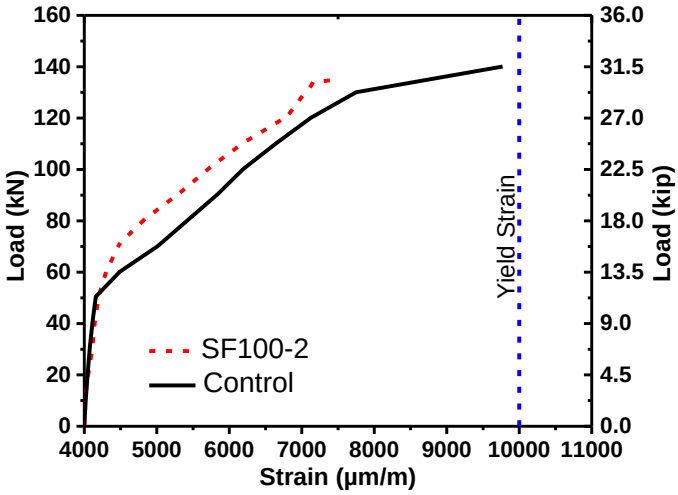

(c) *Strand strain variation in SF100 and SF00*

Fig. 9: *Effect of steel fibers on strain variation of strands in PCB*

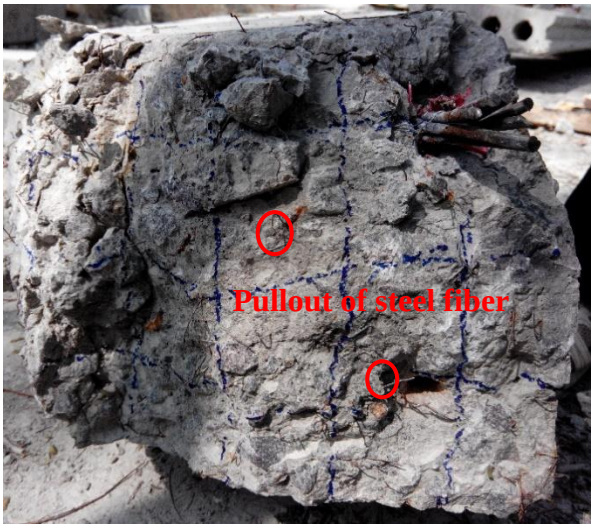

a)*SF35-1*

b) *SF35-2*

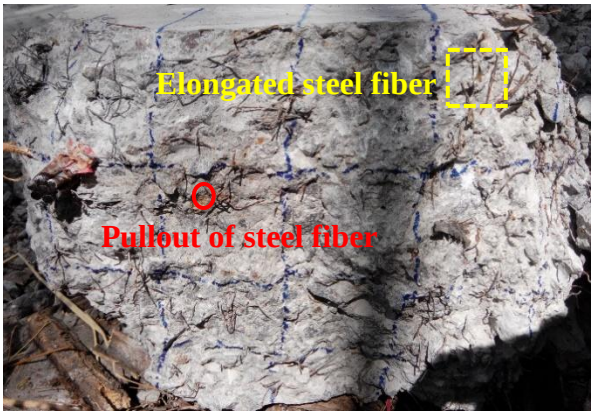

c) *SF70-1*

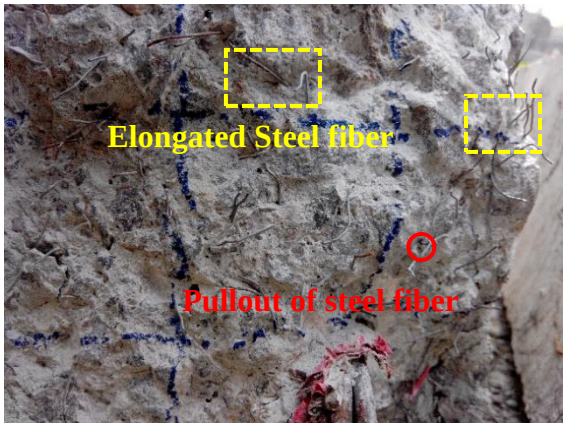

d) *SF70-2*

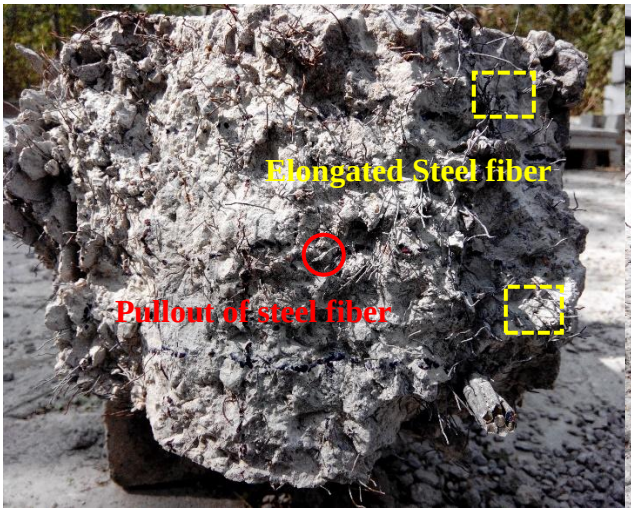

e) *SF100-1*

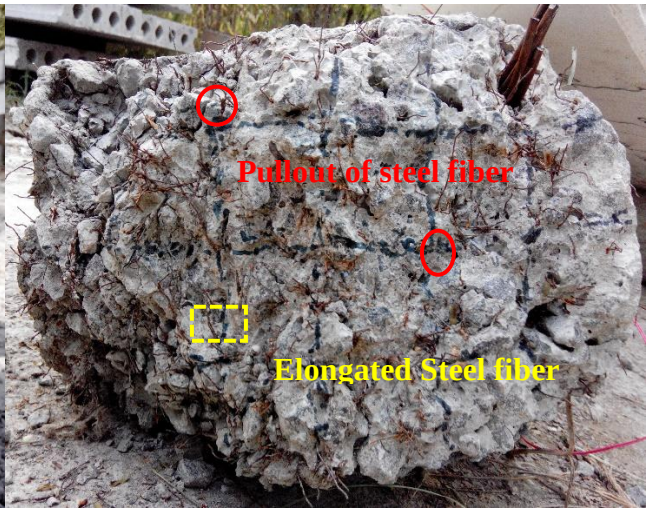

f) *SF100-2*

Fig. 10: *Steel fibers distribution on the failure surface*

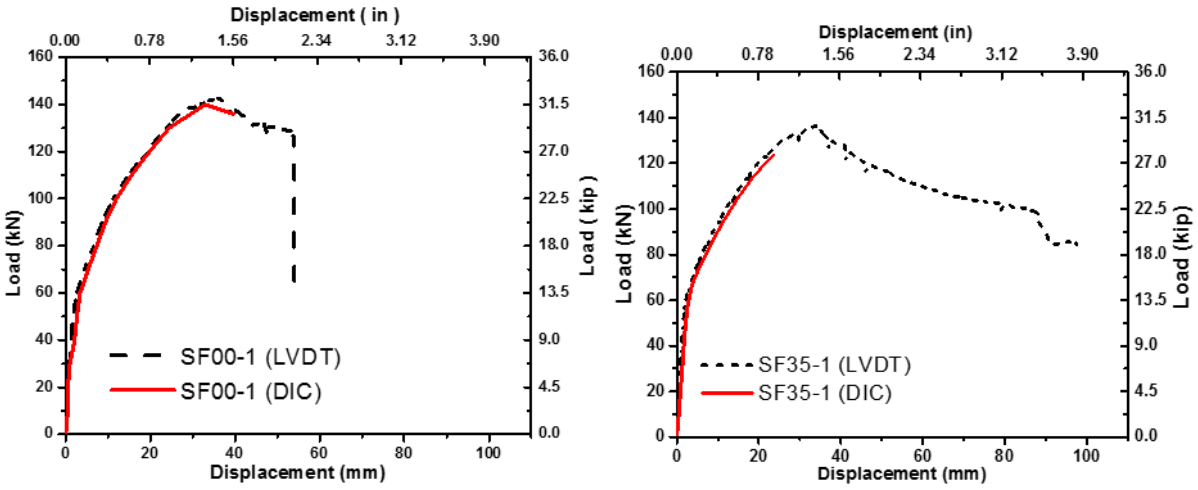

a) *Control specimen (DIC)* b) *PCB with 0.35% steel fibers (DIC)*

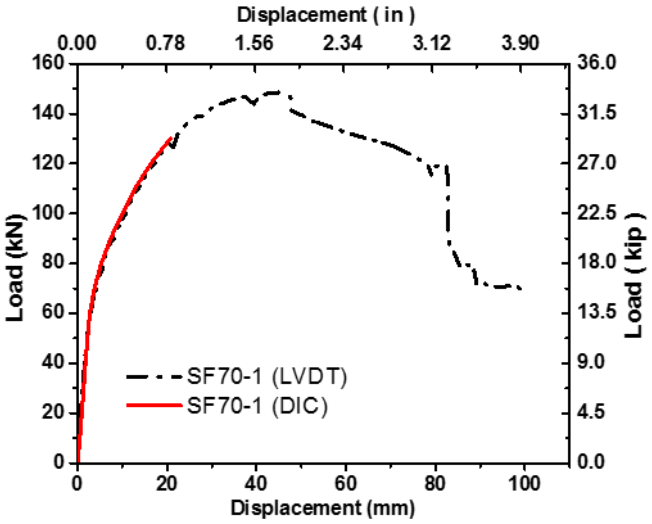

c) *PCB with 0.7% steel fibers (DIC)*

Fig. 11: *Comparison of DIC results with the LVDT measurement*

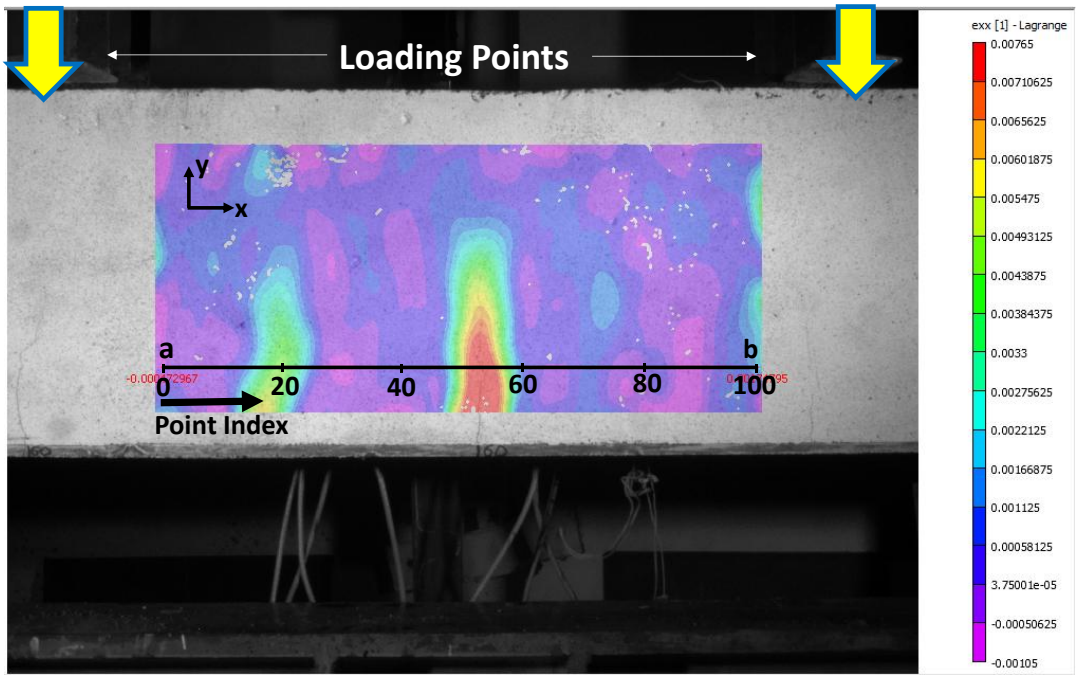

a) *Horizontal line a-b in the tension zone for Analysis (Constant Moment Zone)*

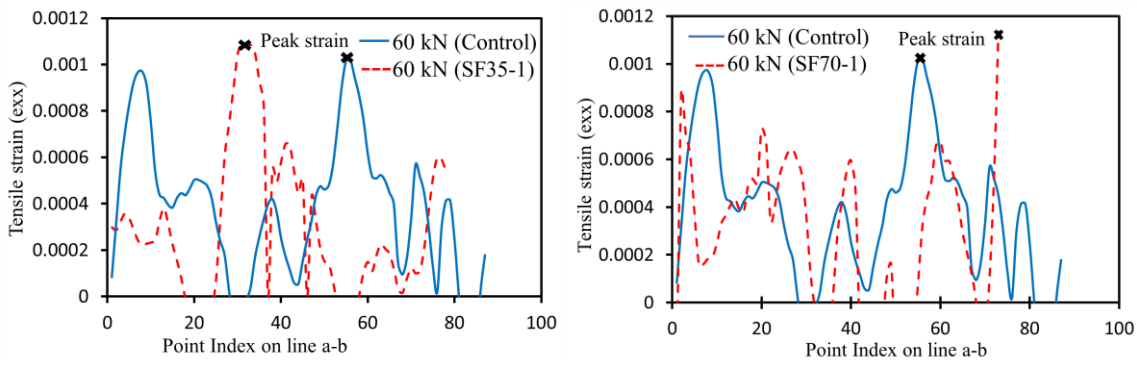

b) *Tensile Strain at 60 kN (13.48 kips) (before cracking)*

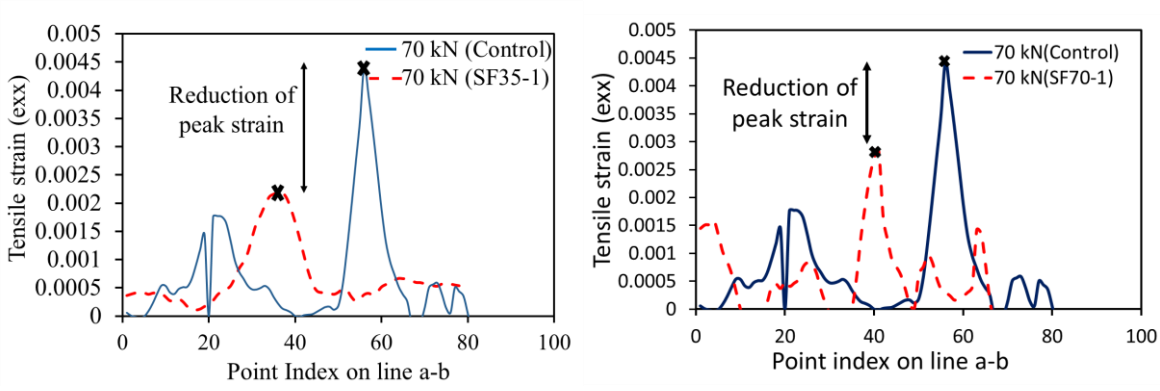

c) *Tensile Strain at 70 kN (15.73 kips) (after cracking)*

Fig. 12: *Longitudinal strain contours (DIC) on the horizontal line a-b before and after cracking*

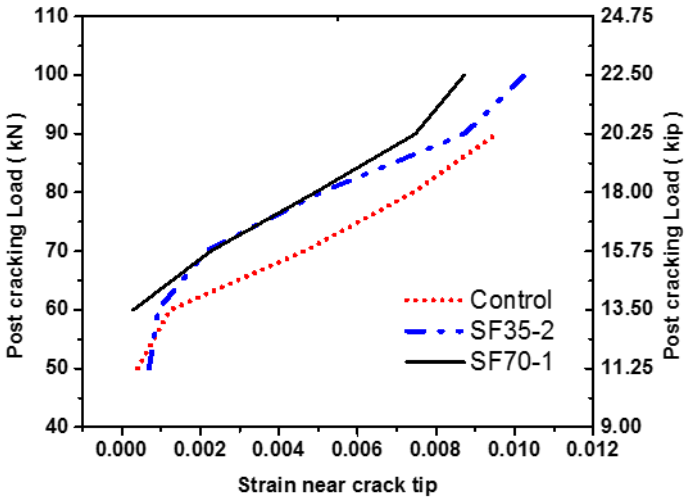

Fig.13: *Average Strain along the level of crack tip at failure*

Control Specimen *SF-0.35%* *SF-0.7%*

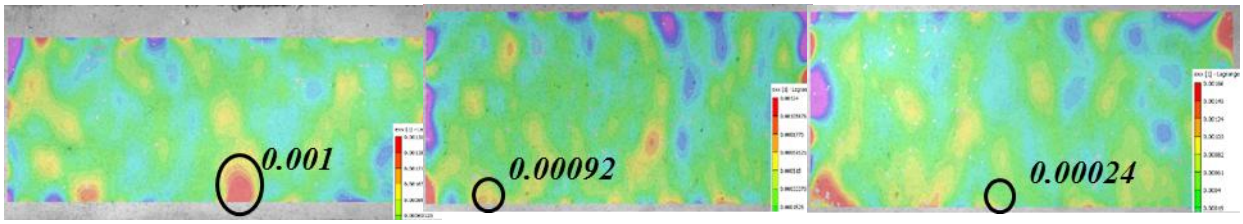

(a) *At a load of 60 kN (13.5 kips)*

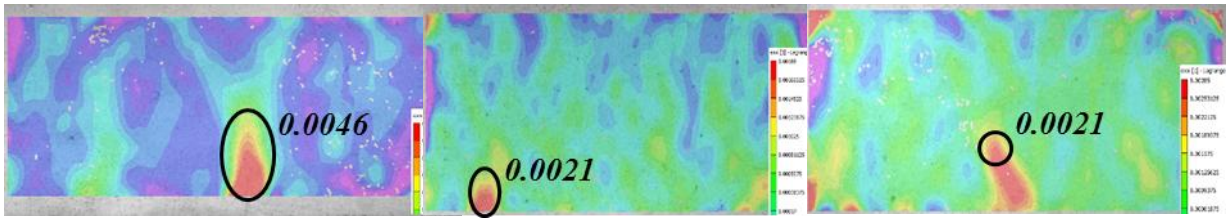

(b) *At a load of 70 kN (15.74 kips)*

(c) *At a load of 80 kN (18 kips)*

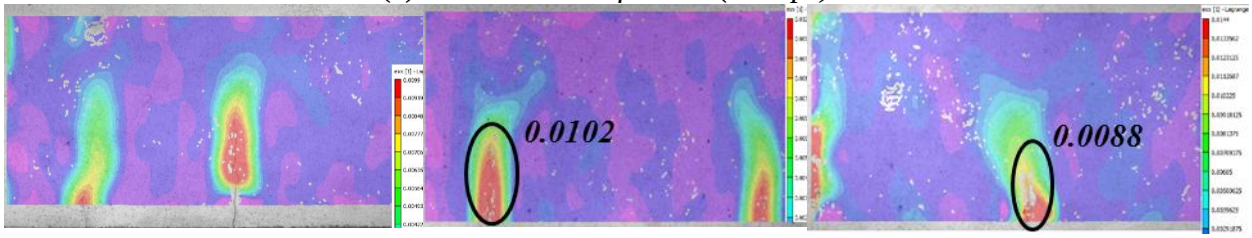

(d) *At a load of 100 kN (22.5 kips)*

Fig. 14: *DIC images showing strain contours at various load levels*

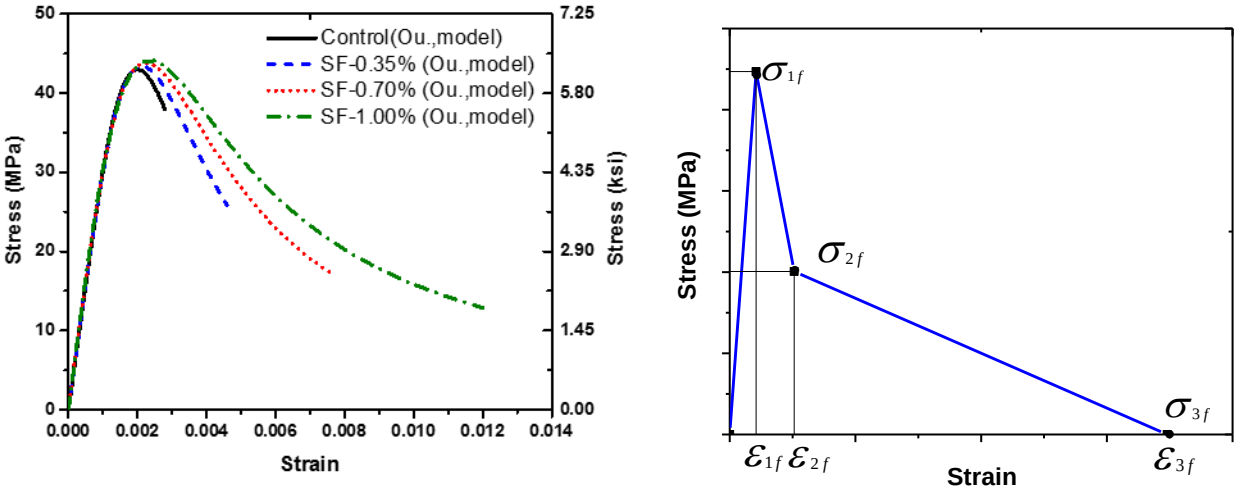

a) Compression behavior prediction *b) Tension behavior prediction*

Fig. 15: *Stress-strain response of fiber-reinforced concrete in compression*[34] *and tension*[35]

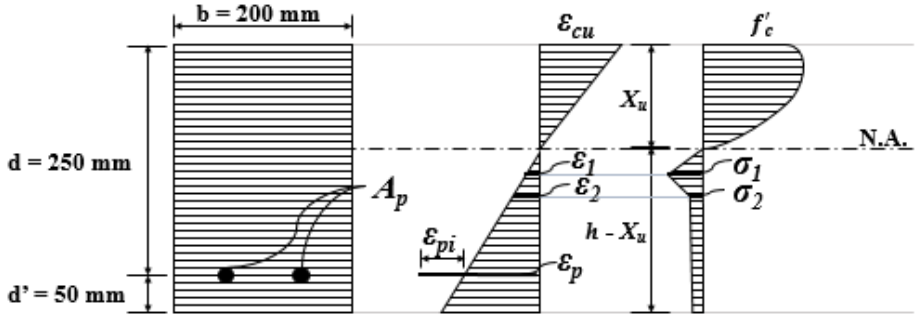

Fig.16*: Layer by layer approach for sectional analysis*

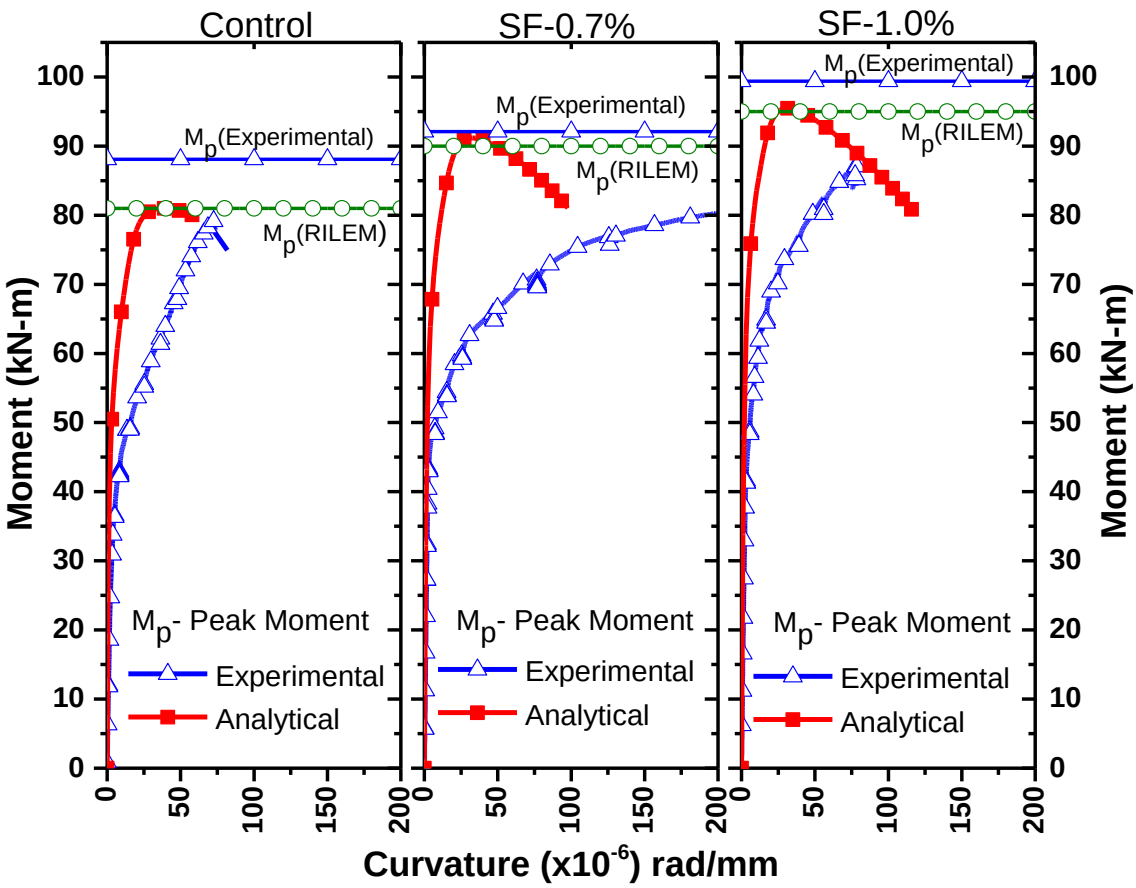

Fig. 17: *Comparison of Analytical and Experimental results (1 kN-m = 0.73576 kip-ft)*